Appl. Phys. B (2016) 122:148
DOI 10.1007/s00340-016-6432-x

Applied Physics B
Lasers and Optics

On the interferometric coherent structures in femtosecond supercontinuum generation

Sirshendu Dinda[1] · **Soumendra Nath Bandyopadhyay**[1] · **Debabrata Goswami**[1]

Received: 7 December 2015 / Accepted: 2 May 2016 / Published online: 11 May 2016

Abstract We report structured interferometric features in femtosecond supercontinuum generation (FSG) with incident laser powers that are near threshold for FSG. We argue that near threshold, these structures arise from the coherent superposition of pulses that are split initially into two daughter pulses during FSG process. Increase in the input pulse energy generates multiple daughter fragments in the temporal domain to an extent that correlated interference structures are not measurable.

1 Introduction

It is a well-known fact that when a very intense ultrashort laser pulse is focused into a transparent dielectric media, the pulse transforms itself into a white supercontinuum (SC) [1]. The SC generated can span the spectrum ranging from IR to UV region [2]. SC generation can be observed in gaseous (air, atmosphere, etc.) [3] and condensed media (glass, calcite, water, CCl_4, etc.) [2, 4, 5]. It has also been studied in waveguides [6] and photonic-crystal fibers [7]. The usefulness of this kind of unique coherent SC light has been exploited in the direction of femtosecond broadband time-resolved spectroscopy [8], optical pulse compression to generate ultrashort pulses [9], detection of pollutants in atmosphere using broadband spectrum LIDAR [10], seed for optical parametric amplification [11], and laser-based precision spectroscopy via the optical frequency comb technique [12, 13].

✉ Debabrata Goswami
dgoswami@iitk.ac.in

[1] Indian Institute of Technology Kanpur, Kanpur 208016, India

Mechanism of SC generation is not fully understood as at such high laser powers interplay among several competing mechanisms occurs. Self-phase modulation (SPM) [2, 5, 7, 14, 15] associated with self-focusing is considered to be the trigger for the drastic broadening of ultrashort pulses. The intensity-dependent "induced Kerr-nonlinearity" of the dielectric medium and the beam shape causes the self-focusing. As an effect of SPM ultrafast pulses gets modulated and broadened, however, this alone cannot explain the nature of SC. Propagation of high-intensity ultrafast laser pulses in the dielectric transparent media to result in the SC pulses elucidates the most significant mechanisms of nonlinear optical ultrafast pulse transformation, namely the ionization-induced SPM, four-wave mixing, SPM enhanced by self-steepening [2, 7], etc. Multiphoton ionization leads to generation of free electrons, which contributes negatively to the refractive index and ultimately stops self-focusing by canceling the Kerr index. Plasma generation occurs due to ionization from multiphoton absorption of the medium from valence band to its conduction band under intense laser radiation. Optical filamentation is the result of the two competing factors: Kerr self-focusing of the laser pulses and the defocusing effect due to plasma generation [17]. This filamentation process is usually accompanied by a broadening of the input laser spectrum and conical emission, which have been extensively investigated in theory and experiments [16–18].

In the supercontinuum generation process, an intense femtosecond pulse propagates through a dielectric (dispersive) medium inducing nonlinear polarization in the medium. This induced polarization in addition to normal GVD and multiphoton ionization results in the spatiotemporal self-focusing, which causes pulse break down. [19, 20]. As the power of the propagating pulse increases, it incorporates more and more chirp in the pulse. Eventually,

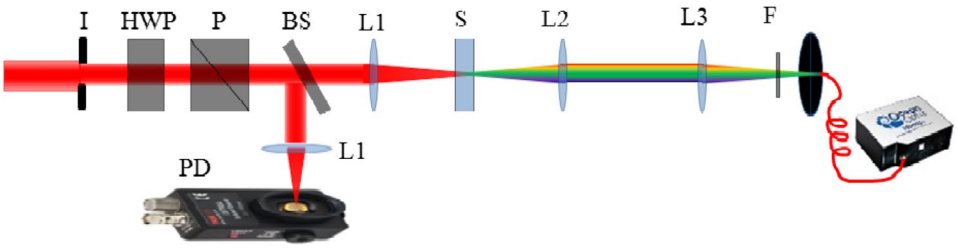

Fig. 1 Experimental setup: *I* iris, *HWP* half-wave plate, *P* polarizer, *L1*, *L2*, and *L3* lenses, *S* sample cuvette, *F* filter

the pulse temporally breaks down to daughter pulses. As all the process involving this breakdown is invoked by nonlinear interaction, the splitting is called nonlinear pulse splitting. The chirp is highly nonlinear, and the central frequency of the leading pulse is downshifted from the initial frequency of the parent pulse. They are also narrower than the parent pulse. Rather than an immediate splitting of the daughter pulses, further increase in input energy replenishes central region of the split pulse. The central region again undergoes split pattern [20, 21]. The pulse can also split in spatial domain. This kind of splitting was first observed in water by Lamb's group [22], where they have used 120-fs pulse (centered at 800 nm). Spatial splitting give rise to two separate SC sources which acts as Young's slit and give rise to spatial fringes. Spatial splitting has also been measured and characterized in BaF_2 [23]. The split sources which have been generated in different media are all mutually coherent as they show spatial interference pattern [22, 24].

For better use of SC, we need to know how to control SC. In our group, we have shown that polarization of the incident pulse plays a critical role in the formation of SC [25–27] in isotropic and anisotropic medium, where we have shown that SC generation is suppressed with circularly polarized. Band gap of transparent dielectric medium is also a determining factor for SC generation [28]. So for better control, we need to know the mechanism of SC generation. To do that we have used two solvents as SC generation medium: water and carbon tetrachloride (CCl_4). Both of them are widely used. We have used pulse energy close to self-focusing regime and studied the interplay among different mechanism as we increase input laser power.

2 Experimental

The experimental setup for studying the SC generation of water (HPLC grade) and CCl_4 consists of a Ti:sapphire regenerative amplifier (Spitfire Pro, Spectra Physics, USA Inc.), operating at 800 nm with 33.7-fs FWHM pulses at 1 kHz repetition rate with pulse energy ~4 mJ. The amplifier is seeded from an integrated Ti:sapphire oscillator pumped by the second harmonic of a continuous wave (cw) Nd:YVO_4 laser, resulting in the femtosecond seed pulses with central wavelength of 810 nm and a spectral bandwidth of 60 nm FWHM at 84 MHz repetition rate at an average power of 650 mW (Maitai, Spectra Physics). The oscillator output is stretched and then fed into the Ti:sapphire regenerative amplifier, which is pumped by the second harmonic of a pulsed Nd:YAG laser operating at a 1 kHz repetition rate (Empower, Spectra physics). The amplifier can also be operated at different repetition rate with same output pulse energy as 1 kHz. We have operated it at 250 Hz.

Using an 80:20 beam splitter and through a mechanical iris, only the central portion of the laser beam with less than 10 % of the 800-nm pulsed light was taken from the Spitfire Pro (Fig. 1). The light was then passed through a half-wave plate (QWPO-800-15-2-AS20) and polarizer combination (Fig. 1) for input intensity attenuation and polarization direction of the beam. Aperture (1 cm diameter) is used to ensure that the beam is almost Gaussian (spatially) and fitting into the entrance of polarizer. The size of the aperture is very critical, as depending on the focusing lens (image plane), the aperture can introduce circular fringes which will alter the SC [29]. This beam is then split into two parts using a wedge beam splitter. One part of the beam is collected in a calibrated photodiode (DET10A/M, Thor Lab) and displayed in a 600-MHz digital oscilloscope (LeCroy 6100A), and other part is focused into the sample (water or CCl_4 in 1 cm quartz cuvette) using 5-cm lens. The SC generated from the sample is then collected by collimating and focusing it to a spectrometer (Ocean Optics, USB4000, 0.2-nm resolution) via another lens and filtering 800-nm light by a suitable filter.

3 Results and discussion

We have acquired SC spectra of water and CCl_4 at 250-Hz repetition rate while changing the input energy of the laser pulse. The collected spectra are average of 10 shots. The amplified pulse has a pulse width of 33.7 fs and a transform limited bandwidth of ~27 nm (Gaussian pulse). As we increased the input energy of the pulse, we started to see the SC in both water and CCl_4 (Figs. 2, 3). In both cases, outcome SC is asymmetric with respect to input 800 nm. Both of them show an anti-Stokes broadening. With

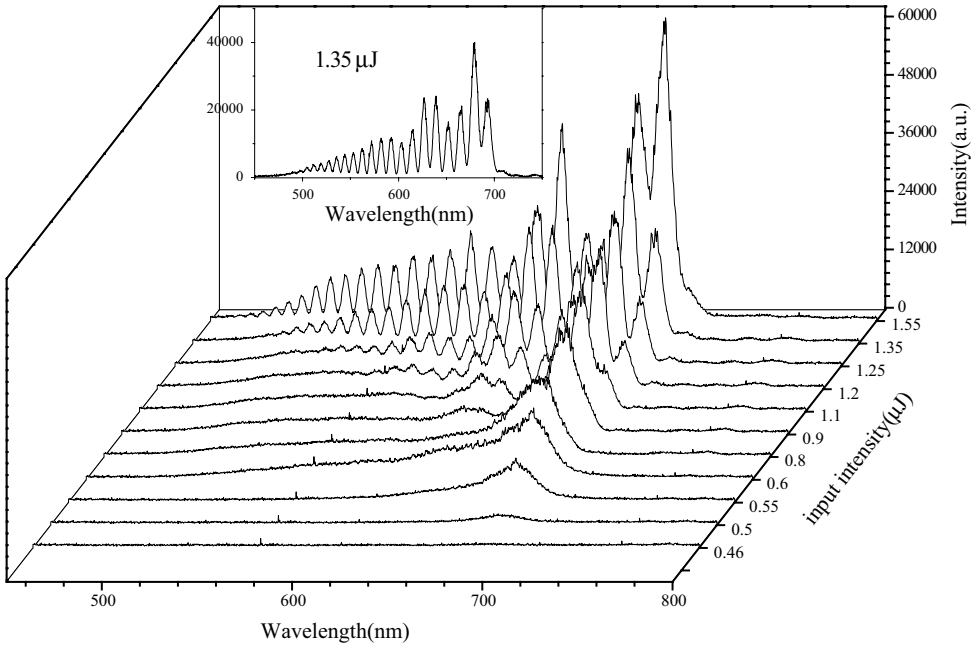

Fig. 2 Supercontinuum spectrum recorded at different input powers for water. At 0.5 μJ, spectrum starts to appear outside the input laser filter range. At 1.1 μJ, first modulation starts to appear at the 650 nm region. As the input pulse energy increases further modulation spreads further into the blue spectral region. (*inset*) Modulated supercontinuum spectrum of water at 1.35 μJ input laser pulse energy, which shows clear modulation from 500- to 700-nm region

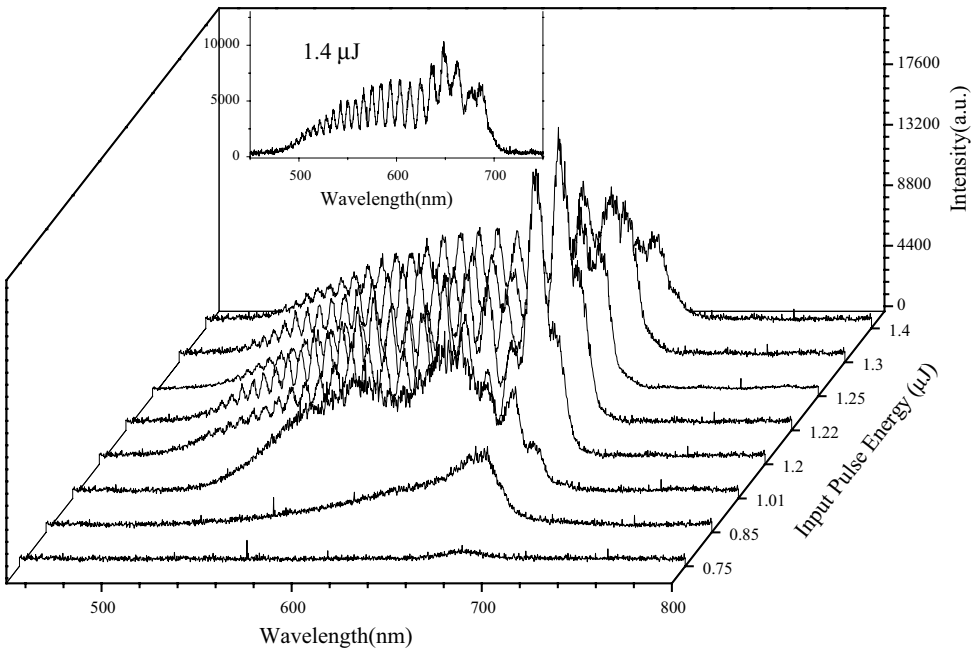

Fig. 3 Supercontinuum spectrum recorded at different input powers for CCl_4. At 0.75 μJ, spectrum starts to appear outside the filter range. (*inset*) Modulated supercontinuum spectrum of water at 1.35 μJ input laser pulse energy, which shows clear modulation from 500- to 700-nm region. The modulation becomes complex after 1.4 μJ input energy due to more than one SC source resulting from multiple pulse splitting

increase in power, both of them go to a maximum broadening. For water, it is 480 nm, and for CCl_4, it is 490 nm. Further increase in power does not increase the bandwidth of the SC but increases the SC intensity. When the input power of the pulse is increased (1.1 μJ for water and 1.05 μJ for CCl_4), output SC starts to exhibit modulated structure. Firstly, the structure appears only in the 700-nm to 650-nm region and the depth of the modulation is very low. With increasing power, the structured pattern spreads throughout the SC band and the depth also increases. Lastly, the spectrum becomes randomly structured after 1.4 μJ (Fig. 3).

Firstly, we will try to understand the asymmetric spectral broadening and halt in the spectral broadening. Self-focusing in almost all media accompanies SC generation. This special feature of self-focusing occurs when input power crosses a critical power P_{crit} [30],

$$P_{\text{crit}} = \frac{3.77\lambda^2}{8\pi n_0 n_2} \tag{1}$$

where λ is wavelength of the input laser, and n_0 and n_2 are the linear and nonlinear refractive index of the medium. In general, n_2 is of the order ~10^{-16} cm^2/W and the SC

generation correlates mainly with the optical Kerr effect and plasma formation [28, 31] by multiphoton absorption (MPA) at higher intensities. Both of these phenomena change the nonlinear refractive index in the medium, which is given by:

$$\Delta n \approx n_2 I(\boldsymbol{r},t) - \frac{2\pi e^2 N_e(\boldsymbol{r},t)}{m_e \omega_0^2} \tag{2}$$

where n_2 is nonlinear refractive index of medium, ω_0 is the optical carrier frequency and m_e is the mass of electron. $N_e(\boldsymbol{r},t)$ is the number of free electrons generated, which depends on the rate of the multiphoton excitation and is represented as:

$$N_e(\boldsymbol{r},t) \approx N_0 w(\boldsymbol{r}) \int_{-\infty}^{t} I^p(\boldsymbol{r},t)\mathrm{d}t \tag{3}$$

where N_0 is the number of initially present neutral particle in the focal volume and p is the number of photon absorbed by the process. First term in right-hand side of Eq. (2) is due to optical Kerr effect, and the second term is due to plasma formation. According to the nonlinear phase $\Delta\varphi = \Delta nkz$, spectral broadening can be written as:

$$\Delta\omega = -\frac{\partial\Delta\varphi}{\partial t} = -\frac{\omega_0 n_2 z}{c}\frac{\partial I(\boldsymbol{r},t)}{\partial t} + \frac{2\pi e^2 z}{m_e \omega_0 c}\frac{\partial N_e(\boldsymbol{r},t)}{\partial t} \tag{4}$$

where z is the propagation distance in medium and k is wave vector. The $\Delta\omega$ consists of positive and negative terms. Positive $\Delta\omega$ term, which corresponds to the anti-Stokes broadening, appears as a result of the contribution from plasma generation at higher intensities.

In any dielectric medium, Δn strictly depends on the intensity of the propagating field. The intensity profile (envelop) of the field creates an inhomogeneous n_2 distribution in the temporal domain. This inhomogeneity of n_2 influences the group velocity of the propagating pulse. In a medium with positive n_2, this nonlinearity causes the group velocity near the edges of the pulse larger than the group velocity of peak. The peak of the pulse under these conditions propagates more slowly than its edges, making the trailing edge of the pulse steeper and reducing the slope of the leading edge, creating a spike in the intensity envelop [28]. The appearance of free electrons by MPA during the intensity spike stimulates a sudden negative index change and thus a sudden drop in nonlinear phase. This translates into a large anti-Stokes broadening in SC [28, 31]. Sudden stop in the broadening pattern in SC at high power indicates that the multiphoton ionization, causing the generation of free electrons, reaches to its equilibrium (intensity clamping) [32].

Now, we will explain the modulation in the spectral pattern, and the information these modulation pattern bears. The modulation of the SC spectrum comes from the interference

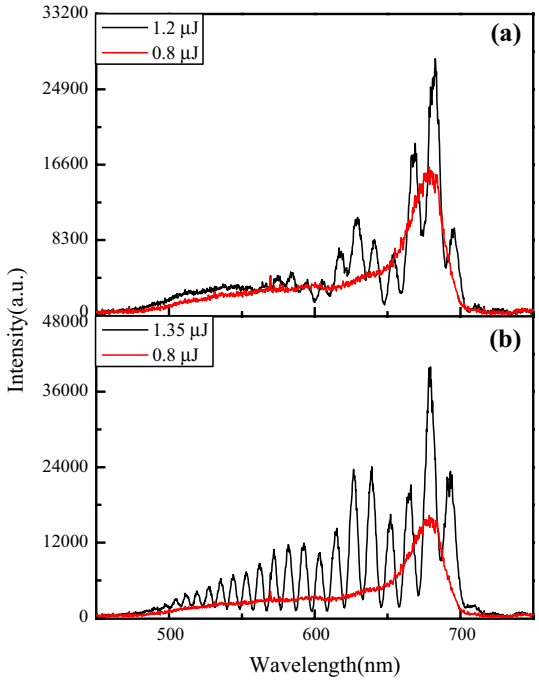

Fig. 4 Supercontinuum spectra of water at different input powers. At lower power, single source emits continuum, and at higher power (1.2 μJ), second source has been generated and it interferes with other source give rise to modulation in spectrum

between two SC sources which are temporally apart from each other due to the nonlinear pulse splitting. Bellini's group has shown that when two time-correlated pulses are collinearly sent through nonlinear medium, the generated SC starts to interfere and give rise to interference structure [33, 34] which is quite similar to the modulation we have got from our SC generated both in water and CCl_4. The pulses can split spatially also and can give rise to Young's fringes which has been studied earlier [22]. We have recorded the spectral modulation of SC at the far field which conveys information about temporal splitting of the pulse. The pulse splits into two daughter pulses when it propagates in dispersive media, as has been shown in experiments and in the theoretical model using nonlinear Schrodinger equation (NLSE) [18, 19, 21]. In Fig. 4, we have represented supercontinuum spectra generated in water at different input power 1.35, 1.2 and 0.8 μJ. At lower power, single source emits continuum, and at higher power (1.2 μJ), 2nd source has been generated and it interferes with other source. The modulation in the continuum spectrum does not spread throughout visible range because the 2nd source does not contain wavelength in the region 450–550 nm. But in the 1.35 μJ case, 2nd source contains all the wavelength of 1st source and the modulation due to interference can be seen clearly. However, it is important to note that the modulated spectra grossly follow the overall intensity profile of the unmodulated spectra (0.8 μJ).

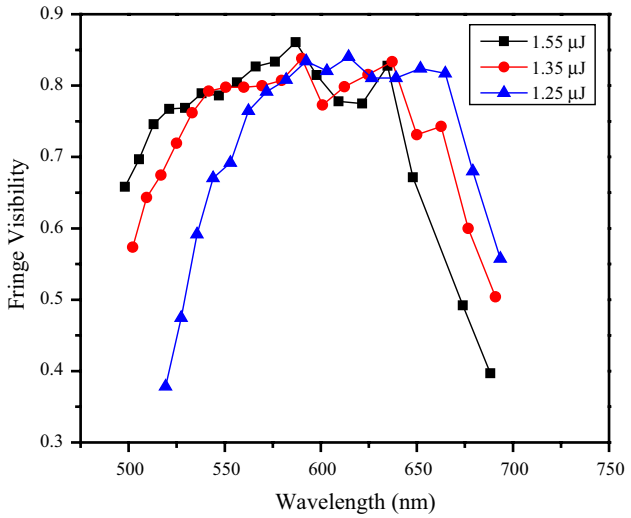

Fig. 5 Fringe visibility for water at different input powers. Visibility falls above 650 nm, because of the use of filter and the tremendous nonlinearity created by the 800-nm pump pulse. Visibility again falls as we move toward the blue spectral region because of the second source

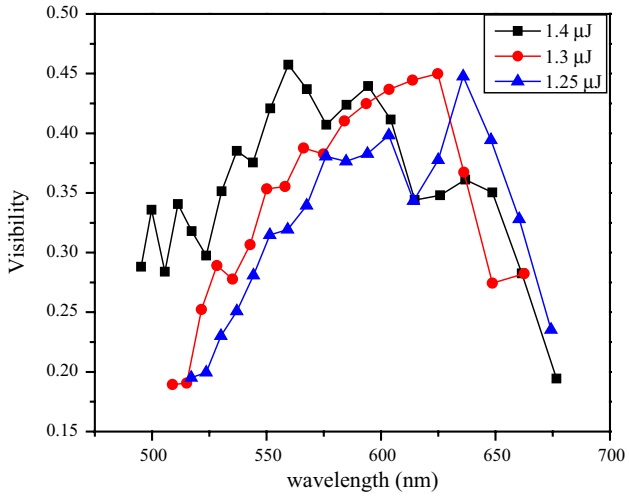

Fig. 6 Fringe visibility for CCl_4 at different input powers. Visibility is sufficiently lower than water as the second source is quite low

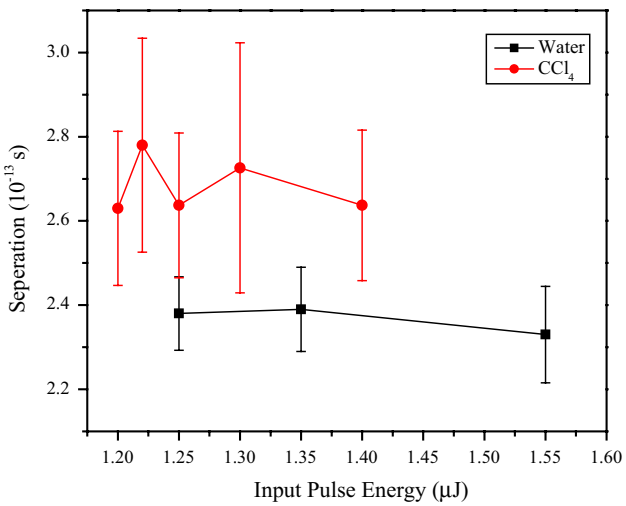

Fig. 7 Separation between split part of water and CCl_4 at different powers of input pulse. The separation remains almost same at different powers for both the cases

In our case, when pulse energy reaches to 1.1 μJ (for water), the femtosecond short pulses fall apart immediately after the pulse self-focusing, creating two different SC sources $U_1(t)$ and $U_2(t+\tau)$. The outcome SC is the superposition of these two sources $U_{SC}(t)$ [35].

$$\begin{aligned} U_{\mathrm{SC}}(t) &= U_1(t) + U_2(t+\tau) \\ &= E_1(t)\exp[i(\omega t + \varphi_1(t)] \\ &\quad + E_2(t)\exp[i\{\omega(t+\tau) + \varphi_2(t)\}] \end{aligned} \tag{5}$$

$\varphi_1(t)$ and $\varphi_2(t)$ are the phases of the two different sources. When $(\varphi_1(t) - \varphi_2(t))$ is constant, sources are mutually coherent and I_{SC} is the intensity output of the SC.

$$\begin{aligned} I_{\mathrm{SC}} &= \left\langle U_{\mathrm{SC}}(t)U_{\mathrm{SC}}^*(t)\right\rangle \\ &= \left\langle U_1(t)U_1^*(t)\right\rangle + \left\langle U_2(t)U_2^*(t)\right\rangle \\ &\quad + \left\langle U_1(t)U_2^*(t+\tau)\right\rangle + \left\langle U_1^*(t)U_2(t+\tau)\right\rangle \end{aligned} \tag{6}$$

$<U_1(t)U_2^*(t+\tau)>$ and $<U_1^*(t)U_2(t+\tau)>$ are mutual coherence function, $\Gamma(\tau)$, and represent temporal complex cross-correlation between the two sources which are separated by τ. Γ_1 and Γ_2 are autocorrelation function of source 1 and 2. So complex degree co-coherence between the sources is given by $\gamma(\tau)$.

$$\gamma(\tau) = \frac{\Gamma(\tau)}{\sqrt{\Gamma_1}\sqrt{\Gamma_2}} \tag{7}$$

Properties of $\gamma(\tau)$ are: its value lies between 0 and 1, and it is proportional to the contrast or visibility of the fringes. Thus, measuring the visibility of the fringes will tell about the quality of the sources in the interference system. Visibility (V) of water and CCl_4 for different power is represented in Figs. 5 and 6. In case of water, the visibility of the fringes is much higher than that of CCl_4. For water, the visibility of fringes at the blue spectrum region increases as we increase the input energy. This is because the second source gains enough energy that it starts to emit light of higher frequency. In case of CCl_4, visibility of fringes is not as much as that of water indicating that in CCl_4, and the second source does not get as much energy as the first source. Moreover, before the optimal value is reached, the pulse in CCl_4 further breaks down removing the interference pattern.

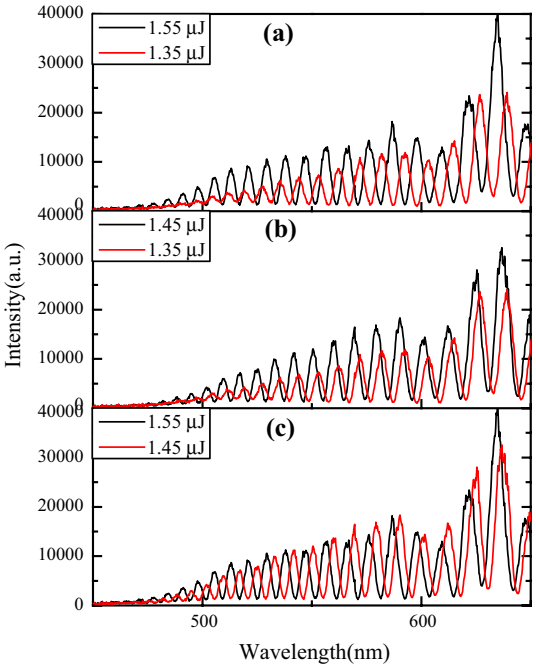

Fig. 8 Enhanced modulation FSG spectra of water for: **a** 1.55 and 1.35 μJ spectra which show a π/2 phase mismatch at ~600 nm. **b** 1.55 μJ and **c** 1.45 μJ spectra, which show π/2 phase mismatch at ~525 nm

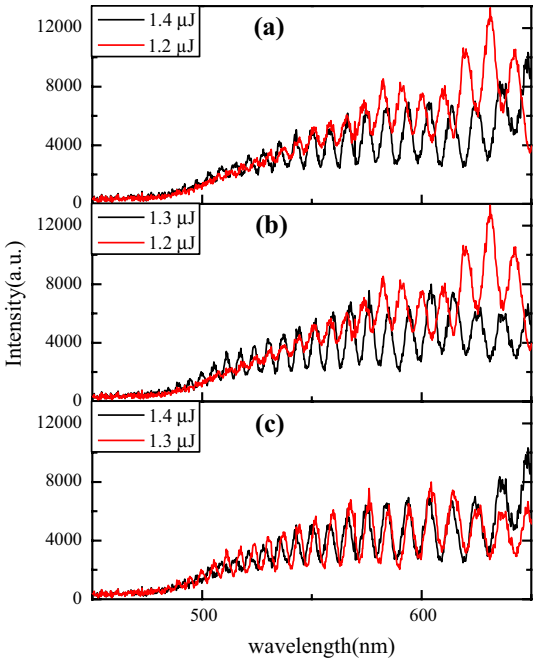

Fig. 9 Enhanced modulation spectra of CCl_4 for: **a** 1.4 and 1.2 μJ spectra which show a π/2 phase mismatch at ~625 nm. **b** 1.3 μJ and **c** 1.2 μJ spectra, which show π/2 phase mismatch at ~625 nm

Separation between split parts, τ, directly related to the bandwidth of the modulated spectra δλ by the relation,

$$\tau = \frac{\lambda^2}{c \times \delta\lambda} \tag{8}$$

which leads to the separation for water as ~240 fs and for CCl_4 ~270 fs (Fig. 7). Both GVD and band gap for water and CCl_4 are different. GVD of water is 24.76 fs^2/mm (for 800 nm propagation) and that of CCl_4 is 63.1 fs^2/mm [36]. Band gap of water is 7.5 eV and that of CCl_4 is 4.8 eV [28]. So the separations between two split pulses are different for two distinctively different dispersive media. A small increase in the power does not increase the separation significantly but changes the spectral modulation peaks (Figs. 8, 9). Shift in spectral modulation peaks proves that at different inputs, the split parts have different phases as compared to the previous one. Since the trailing part propagates through medium, it is transformed with respect to the leading split part. Further increase in laser power continually leads to increased number of sub-pulses, which eventually reduces the modulatory behavior of the SC generation for well beyond threshold condition.

4 Conclusion

Delicate interference structure appears in the supercontinuum in water and CCl_4 as the energy of the input pulse crosses the threshold value of 1 μJ. Thereafter, the input pulse splits into two sub-pulses separated by ~240 fs in water and ~270 fs in CCl_4. The fringe pattern in the SC spectrum shows that with an increase in input pulse energy, the sub-pulses take different temporal phases, though their temporal separation remains almost constant. Finally, increase in the input pulse energy well beyond threshold of SC results in simultaneous generation of multiple daughter fragments such that no correlated interference structures are measurable.

Acknowledgments We acknowledge the financial supports from the Department of Science and Technology (DST), Ministry of Human Resource and Development (MHRD), Indian Space Research Organization (ISRO), and University Grants Commission (UGC), India. Additionally, we thank Ms. S. Goswami for language corrections in the manuscript.

References

1. R.R. Alfano, S.L. Shapiro, Emission in the region 4000–7000 Å via four-photon coupling in glass. Phys. Rev. Lett. **24**, 584–587 (1970)
2. R.R. Alfano, *The Supercontinuum Laser Source* (Springer, New York, 2006)
3. P.B. Corkum, C. Rolland, Supercontinuum generation in gases. Phys. Rev. Lett. **57**, 2268–2271 (1986)
4. V. Kartazaev, R.R. Alfano, Supercontinuum generated in calcite with chirped femtosecond pulses. Opt. Express **32**, 3293 (2007)

5. W. Lee Smith, P. Liu, N. Bloembergen, Superbroadening in H_2O and D_2O by self-focused picosecond pulses from a YAlG: Nd laser. Phys. Rev. A **15**, 2396 (1977)
6. M.A. Foster, A.L. Gaeta, Ultra-low threshold supercontinuum generation in sub-wavelength waveguides. Opt. Express **12**, 3137–3143 (2004)
7. A.M. Zheltikov, Let there be white light: supercontinuum generation by ultrashort laser pulses. Phys.-Usp. **49**, 605–628 (2006)
8. S.A. Kovalenko, A.L. Dobryakov, J. Ruthmann, N.P. Ernsting, Femtosecond spectroscopy of condensed phases with chirped supercontinuum probing. Phys. Rev. A **59**, 2369–2384 (1999)
9. E.T.J. Nibbering, O. Dühr, G. Korn, Generation of intense tunable 20-fs pulses near 400 nm by use of a gas-filled hollow waveguide. Opt. Lett. **22**, 1335–1337 (1997)
10. P. Rairoux, H. Schillinger, S. Niedermeier, M. Rodriguez, F. Ronneberger, R. Sauerbrey, B. Stein, D. Waite, C. Wedekind, H. Wille, L. Wöste, C. Ziener, Remote sensing of the atmosphere using ultrashort laser pulses. Appl. Phys. B **71**, 573–580 (2000)
11. V.V. Yakovlev, B. Kohler, K.R. Wilson, Broadly tunable 30-fs pulses produced by optical parametric amplification. Opt. Lett. **19**, 2000–2002 (1994)
12. J. L. Hall, T. W. Hänsch, The development of laser-based precision spectroscopy, including the optical frequency comb technique, http://www.nobelprize.org/nobel_prizes/physics/laureates/2005/
13. S.T. Cundiff, J. Ye, Colloquium: femtosecond optical frequency combs. Rev. Mod. Phys. **75**, 325 (2002)
14. A.L. Gaeta, Catastrophic collapse of ultrashort pulses. Phys. Rev. Lett. **84**, 3582–3585 (2000)
15. G. Yang, Y.R. Shen, Spectral broadening of ultrashort pulses in a nonlinear medium. Opt. Lett. **9**, 510–512 (1984)
16. R.R. Alfano, P.P. Ho, Self-, cross-, and induced-phase modulations of ultrashort laser pulse propagation. Quant. Electron. **24**, 351–364 (1988)
17. A. Couairona, A. Mysyrowicz, Femtosecond filamentation in transparent media. Phys. Rep. **441**, 47–189 (2007)
18. K.D. Moll, A.L. Gaeta, Role of dispersion in multiple-collapse dynamics. Opt. Lett. **29**, 995–997 (2004)
19. J.K. Ranka, R.W. Schirmer, A.L. Gaeta, Observation of pulse splitting in nonlinear dispersive media. Phys. Rev. Lett. **77**, 3783 (1996)
20. M. Kolesik, E.M. Wright, J.V. Moloney, Dynamic nonlinear X waves for femtosecond pulse propagation in water. Phys. Rev. Lett. **92**, 253901 (2004)
21. J.K. Ranka, A.L. Gaeta, Breakdown of the slowly varying envelope approximation in the self-focusing of ultrashort pulses. Opt. Express **23**, 534 (1998)
22. K. Cook, A.K. Kar, R.A. Lamb, White-light supercontinuum interference of self-focused filaments in water. Appl. Phys. Lett. **83**, 3861 (2003)
23. A.K. Dharmadhikari, J.A. Dharmadhikari, D. Mathur, Visualization of focusing–refocusing cycles during filamentation in BaF_2. Appl. Phys. B **94**, 259 (2009)
24. W. Watanab, K. Itoh, Spatial coherence of supercontinuum emitted from multiple filaments. Jpn. J. Appl. Phys. **40**, 592 (2001)
25. A.S. Sandhu, S. Banerjee, D. Goswami, Suppression of supercontinuum generation with circularly polarized light. Opt. Commun. **181**(1), 101–107 (2000)
26. A. Srivastava, D. Goswami, Control of supercontinuum generation with polarization of incident laser pulses. Appl. Phys. B **77**(2–3), 325–328 (2003)
27. S. Dinda, D. Goswami, On the generation and control of femtosecond supercontinuum. Sci. Lett. **4**, 137 (2015)
28. A. Brodeur, S.L. Chin, Band-gap dependence of the ultrafast white-light continuum. Phys. Rev. Lett. **80**, 4406–4409 (1998)
29. K. Cook, A.K. Kar, R.A. Lamb, White-light filaments induced by diffraction effects. Opt. Express **13**, 2025 (2005)
30. J.H. Marburger, Self-focusing: theory. Prog. Quant. Electron. **4**, 35 (1975)
31. V.P. Kandidov, O.G. Kosareva, I.S. Golubtsov, W. Liu, A. Becker, N. Akozbek, C.M. Bowden, S.L. Chin, Self-transformation of a powerful femtosecond laser pulse into a white-light laser pulse in bulk optical media (or supercontinuum generation). Appl. Phys. B **77**, 149–165 (2003)
32. W. Liua, S. Petita, A. Beckera, N. Aközbekb, C.M. Bowdenb, S.L. Chin, Intensity clamping of a femtosecond laser pulse in condensed matter. Opt. Commun. **202**, 189–197 (2002)
33. C. Corsi, A. Tortora, M. Bellini, Mutual coherence of supercontinuum pulses collinearly generated in bulk media. Appl. Phys. B **77**, 285 (2003)
34. A. Tortora, C. Corsi, M. Bellini, Comb-like supercontinuum generation in bulk media. Appl. Phys. Lett. **85**, 1113 (2004)
35. M. Born, E. Wolf, *Principles of Optics*, 7th edn. (Cambridge University Press, Cambridge, 1999)
36. P. Devi, V.V. Lozovoy, M. Dantus, Measurement of group velocity dispersion of solvents using 2-cycle femtosecond pulses: experiment and theory. AIP Adv. **1**, 032166 (2011)